Environmental Science: Atmospheres

ROYAL SOCIETY OF CHEMISTRY

PAPER

View Article Online
View Journal | View Issue

Cite this: *Environ. Sci.: Atmos.*, 2024, **4**, 802

Formation of secondary aerosol from emissions of a Euro 6d-compliant gasoline vehicle with a particle filter†

Andreas Paul, *[ad] Zheng Fang,[b] Patrick Martens,[d] Arya Mukherjee,[e] Gert Jakobi,[c] Mika Ihalainen,[e] Miika Kortelainen,[e] Markus Somero,[e] Pasi Yli-Pirilä,[e] Thorsten Hohaus, *[a] Hendryk Czech,[cd] Markus Kalberer,[f] Olli Sippula,[eg] Yinon Rudich,[b] Ralf Zimmermann[cd] and Astrid Kiendler-Scharr ‡[a]

The most recent European regulation, the Euro 6d emission standard, requires all gasoline direct injection (GDI) vehicles to use both a three-way catalyst (TWC) and a gasoline particle filter (GPF) as exhaust aftertreatment. These aftertreatment methods are aimed at reducing NO_x and primary particle emissions. However, the formation of secondary organic aerosols (SOAs) from the volatile organic compound (VOC) emissions of a Euro 6d compliant GDI vehicle, factory equipped with a GPF is not yet investigated. Therefore, to explore the SOA formation and effects of the GPF, the exhaust of a Euro 6d compliant GDI vehicle was characterized at 4 different steady state speeds, idling (0 km h^{-1}), 50, 80 and 100 km h^{-1}. The exhaust was oxidised in a photochemical emission aging flow tube reactor (PEAR) by reactions with OH radicals equivalent of 2.2 days of atmospheric day time oxidation. It was found that the GPF completely removes primary particles larger than 10 nm, at all investigated vehicle speeds. However, significant SOA was formed after oxidation, with the highest SOA formation potential per kg fuel consumed at 50 km h^{-1}. The main SOA precursors were determined to be toluene, xylene and trimethyl-benzene which were found to account for at least 50% of SOA formed at all driving speeds. Furthermore, high emissions of ammonia (NH_3) could be observed in the exhaust under all driving conditions which resulted in the subsequent formation of ammonium nitrate (NH_4NO_3) after aging. The formation of NH_4NO_3 additionally facilitated the co-condensation of organic gas phase products after OH oxidation enhancing SOA mass even further.

Received 24th November 2023
Accepted 3rd June 2024

DOI: 10.1039/d3ea00165b

rsc.li/esatmospheres

Environmental significance

Particulate matter (PM) from gasoline vehicles' exhaust impacts health and urban air quality. Recent studies of PM formation from Euro 6 compliant cars did not include a Gasoline Particle Filter (GPF). As the GPF has become mandatory to remove PM it is critical to understand the fate of the remaining gas phase emissions after atmospheric oxidation. In this study, emissions of a GPF equipped Euro 6 car were aged in an oxidation flow reactor simulating atmospheric photochemistry processing. While primary PM emissions are below the detection limit, emission factors of secondary aerosols formed from organics, NH_3 and NO_x can reach 124 ± 5 mg kg^{-1} fuel. Furthermore, analysis of major organic precursors highlights the importance of the remaining vehicular emissions regarding their aerosol formation potential.

[a]*IEK-8 Troposhere, Forschungszentrum Jülich GmbH, Jülich, 52428, Germany. E-mail: an.paul@fz-juelich.de; t.hohaus@fz-juelich.de*

[b]*Department of Earth and Planetary Science, Weizmann Institute of Science, Rehovot, 7610001, Israel*

[c]*Group of Comprehensive Molecular Analytics, Helmholtz Zentrum München, Neuherberg, 85764, Germany*

[d]*Department of Technical and Analytical Chemistry, University of Rostock, Rostock, 18051, Germany*

[e]*Department of Environmental and Biological Science, University of Eastern Finland, Kuopio, 70210, Finland*

[f]*Department of Environmental Science, University of Basel, Basel, 4056, Switzerland*

[g]*Department of Chemistry, University of Eastern Finland, Joensuu, 80101, Finland*

† Electronic supplementary information (ESI) available. See DOI: https://doi.org/10.1039/d3ea00165b

‡ Astrid Kiendler-Scharr passed away on February 6th, 2023.

Introduction

Atmospheric aerosol has been ranked as the top global environmental health risk[1] having an estimated impact on life expectancy of up to 2.9 years lost on a global scale.[2,3] A clear link between secondary organic aerosol (SOA) and cardiovascular and respiratory diseases has shown that secondary aerosols may be more impactful on human health than primary aerosols.[4] Furthermore, it has been shown that typical anthropogenic SOAs formed from aromatic precursors have a more adverse impact on lung cells.[5] Among others, combustion processes and traffic-related aerosol emissions have been identified as

particularly health-relevant sources of atmospheric aerosol.[6,7] Regulations for vehicle emissions are regularly updated based on new evidence for human health effects and climate impact. With the introduction of the Euro 6 emission standards by the European Union, the total particle number (PN) emitted per km (# km^{-1}) driven from a gasoline direct injection (GDI) vehicle has been limited to 6×10^{11} # km^{-1}. In contrast, the older Euro 5 regulations did not limit the PN per km but placed only an overall limit on the particle mass emitted (up to 4.5 mg km^{-1}), a regulation which still applies to the Euro 6d emission standard. To comply with new regulations, the gasoline particle filter (GPF) has been implemented as a standard exhaust aftertreatment technology for GDI vehicles. The GPF has proven to be efficient at reducing primary aerosol (PA), often achieving a filter efficiency of >90%.[8] Regulations on CO (1000 mg km^{-1}) and NO_x (60 mg km^{-1}) emissions resulted in the introduction of the three-way catalyst (TWC), intended to convert NO_x to N_2, and CO and non-methane hydrocarbons (NMHCs) to CO_2. Furthermore, current standards limit the emission of the total concentration of NMHCs to 68 mg km^{-1} and the total hydrocarbon (THC) emissions to 100 mg km^{-1}.

However, it has been shown that volatile organic compounds (VOCs), particularly single ring aromatics, emitted during driving or idling with a GDI vehicle form significant SOA when oxidized in the atmosphere.[9–12] Nordin *et al.* 2013 and Liu *et al.* 2015 found that 60–90% of SOA formation could be assigned to C6–C10 aromatics for Euro 1–Euro 4 compliant gasoline cars.[13,14] Whilst these are likely Port Fuel Injection (PFI) engines the composition of the gasoline is still comparable. Measurements of the exhaust from Euro 5 cars retrofitted with GPF showed similar results that 96.7% of the gas phase aromatics were composed of C6–C10 aromatics.[11] Roth *et al.* 2019 showed that retrofitting a GPF to a Euro 5 compliant car resulted in significantly reduced primary aerosol, however significant SOA formation was still an important contribution to the total particle mass measured. The GPF has additionally been found to reduce some SOA precursors and thus also SOA formation.[15–17] Furthermore, most studies have focused on dynamic driving cycles such as the L92 or the worldwide harmonized light vehicle test cycle (WLTC) and batch experiments to assess average emissions of a full cycle or cold start emissions. Additionally, emission of NH_3 is particularly important as it is known to enhance new particle formation and increase SOA yields, promoting further nucleation and growth of aerosol from vehicle exhaust.[18–23] Both SOA and NH_3 are currently unregulated although the proposed Euro 7 emission standards[24] aim to limit NH_3 emissions from gasoline vehicles to 20 mg km^{-1}.

Therefore, dedicated experiments are necessary to evaluate the fate of vehicle emissions of modern cars after release into the atmosphere and upon timescale of typical atmospheric aging processes. Various simulation chamber and oxidation flow reactor studies have investigated SOA formation by the oxidation of vehicle emission from older car models *via* reactions with hydroxyl radicals (OH) being the major chemical reaction in the troposphere.[11–16,23,25–29] However, the primary emissions and secondary aerosol formation potential from a Euro 6d personal GDI vehicle with both TWC and GPF as part of the original factory setup are not well known. Additionally, there are only a few experiments conducted on steady state driving from a warm engine start.[25] Therefore, it remains relevant to understand the emissions at different vehicle speeds and the impacts of atmospheric aging on these emissions.

Materials and methods

Emissions of a Euro 6d emission standard compliant Skoda Scala passenger vehicle (model year 2021, factory equipped with a GDI engine, a GPF, and a TWC) were measured. All detailed vehicle specifications are shown in Table S1.† The vehicle was fuelled with 95 E10 gasoline, consisting of 10% ethanol as the biofuel component and connected to a Rototest VPA-RX3 2WD chassis dynamometer, which enabled its operation under steady-state conditions. The duration of the test cycle was set to be in total 60 minutes, comprising of four 15 min long segments evenly distributed to idling, 50 km h^{-1}, 100 km h^{-1} and 80 km h^{-1}. The test cycle was repeated 16 times in 4 experiments, each experiment consisting of 4 uninterrupted consecutive test cycles. The initial test cycle in each experiment is not considered in the analysis of this paper as it represents a cold start of the engine. The remaining 12 warm test cycles have thus been analysed and subsequently averaged ($n = 12$). A detailed overview of the driving cycle is summarized in the supplement (Fig. S1, 2 and Table S2†). All vehicle speeds are equivalent to flat surface driving (Table S3†). For analysis of steady state driving conditions, the initial 5 minutes of driving time for each test cycle segment is excluded to ensure that there are no effects of (de-) accelerations on the steady state measurements.

The experimental setup is illustrated in Fig. 1. The vehicle exhaust pipe was connected to the diluters *via* a heated tubing, consistently heated to 120 °C. A portion of the exhaust flow was sampled and subsequently diluted using a combination of a porous tube diluter and an ejector diluter (DAS; Venacontra, Finland). The dilution process was carefully regulated by

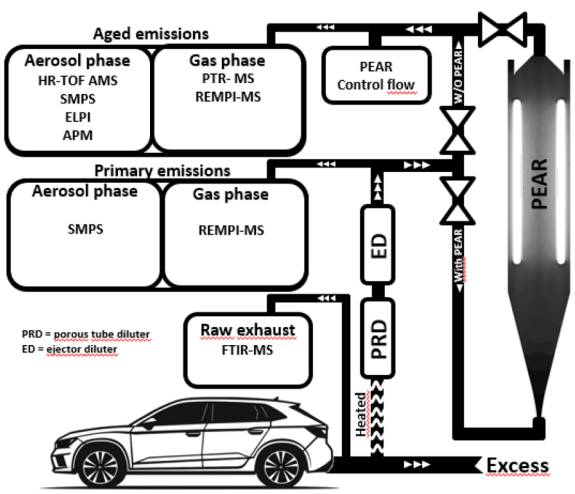

Fig. 1 The setup includes all instruments on the primary emission run without the PEAR, and aged emissions run with the PEAR.

adjusting the flow rate of the porous tube diluter, while maintaining a constant flow rate in the ejector diluter, to achieve a controlled dilution factor of 17. The dilution factor was defined based on the measured CO_2 concentrations before and after the dilution process. Primary gas phase emissions were measured directly at the exhaust with Fourier transform Infrared (FTIR) spectroscopy. The diluted exhaust was drawn into the Photochemical Emission Aging flow tube Reactor (PEAR), operated at a constant flow of 120 l min^{-1}. Based on this flow rate the transmission efficiency of aerosols is estimated to be above 70% for 20 nm aerosols and above 90% above 40 nm.[30] Furthermore, the total dilution in the PEAR was 1 : 18 in relation to the exhaust. Aerosols were measured before (primary emissions) and after the PEAR (aged emissions). Background measurements were preformed prior to each experiment ensuring that no significant aerosol formation (<0.5 μg m^{-3}) occurred in the PEAR. At the entrance of the PEAR, water vapor was added to reach a minimum relative humidity of 40%, which varied between 40% and approximately 65% depending on the driving conditions. OH-radicals were generated inside the PEAR by ozone (7 ppm) and photolysis at 254 nm. The formed singlet oxygen ($O(^1D)$) reacts with water vapor, producing OH radicals which initiates oxidation in the PEAR. Furthermore, some ozonolysis occurs in the PEAR due to the ozone concentration. A proton-transfer-reaction mass spectrometer (PTR-MS-8000; Ionicon, Austria) was used to measure VOCs from the outlet of the PEAR with time resolution of 10 s. The PTR-MS operated in H_3O^+ mode, and an E/N ratio of 137 was reached. 1,3-Diiodobenzene was used as an internal standard for mass calibration, and the mass resolution was ~5000 at m/z 59. The equivalent photochemical age was determined to be on average 3.3 days based on the principle of the "photochemical clock".[31] About 65 ppb of isotope-labelled *N*-butanol (d9-BuOH, 98%, Cambridge Isotope Laboratories) was added to the primary emissions. The decay of d9-BuOH measured by PTR-MS was used to calculate the photochemical age. This calculation is based on a known rate constant of d9-BuOH with OH ($k_{\text{butanol-d9}}$ = 3.4(±0.88) × 10^{-12} cm^3 per molecule per s),[32] assuming an ambient concentration of OH radicals of 1.5 × 10^6 cm^{-3}.[33] To evaluate the relevance of the aging process in the PEAR compared to typical ambient conditions, the oxidation conditions in the OFR were modelled following the approach by Peng *et al.* 2019.[34–38] Due to high concentrations of VOCs, NO and other trace gases in the exhaust, the total external OH reactivity ($OHR_{ext} = \sum k_x c_x$ where c_x is the concentration of an OH-consuming species, x, and k_x the rate constant between x and OH) is high compared to the photolysis rate. This results in conditions in the PEAR that are still reasonably close to ambient oxidation processes but might have contributions from photolysis at 254 nm that are significant (>15%) during idling and 50 km h^{-1} (Table S8†). These conditions are classified as "risky" for typical OFR oxidation processes (details, ESI Tables S4–7†). SO_2 was used as a surrogate for NMHC.[38] Additionally during driving CO emissions cause additional formation of HO_2. Thus, the RO_2 fate pathway during idling, 80 km h^{-1} and 100 km h^{-1} was primarily the HO_2–RO_2 reaction (>80%). Only during the 50 km h^{-1} segment due to high NO emissions did the RO_2 fate pathway change as a significant fraction of the RO_2 reacted with NO (18.1%) with RO_2–OH (68.5%) and RO_2–HO_2 (12.6%) (Table S7†).

Furthermore, the age of the experiment was modelled assuming an OH exposure of 1.5 × 10^6 cm^{-3},[33] the harmonic mean age of the experiment is found to be 1.5 days in comparison to the measured age of 2.2 days, thus the model is a reasonable comparison to the measured age. The idling phase is overestimated in terms of OH exposure, however, calculating an average age of the idling segment is not ideal due to the large dynamic changes that occur during this period, and the measured age varies from 0.5 days (last 5 min) to 5.7 days (first 10 min). Additionally, the model consistently underestimates the exposure at all other driving speeds. Notably, the modelled age is calculated on an $n = 12$ basis and the measured age from an $n = 1$ experiment thus some deviation should be expected (Table S9†).

A resonance-enhanced multi-photon ionization mass spectrometer (REMPI-MS)[39] was alternatingly measuring before and after the PEAR using an 8-port-2-way-valve (VICI; Switzerland) to monitor the changes in aromatic concentrations after aging with 1 minute time resolution. Isotopically labelled toluene (d3-toluene, isotopic purity of 98%; Cambridge Isotope Inc.) was added as an internal standard for quantification.[40] Quantification of aromatic VOC was based on photoionization cross-sections determined by Gehm *et al.* 2018.[41] The aerosol size distributions were measured with a scanning mobility particle sizer (SMPS). Aerosol effective densities were determined using an Aerosol Particle Mass analyser (APM) combined with an SMPS as described by Leskinen *et al.* (2014).[42] The aerosol composition was determined using a High-Resolution Time of Flight Aerosol Mass Spectrometer (HR-ToF AMS). The AMS was operated on an additional 1 : 10 dilution using a similar dilution method to that described above. The AMS gas phase CO_2 was corrected according to CO_2 measurements using a Vaisala CO_2 sensor, measuring directly at the AMS inlet. The PM1 aerosol mass concentrations were separated into organics (org), NH_4, NO_3 and SO_4 using the AMS. Additionally, the AMS was used to determine the elemental composition in terms of the ratio of oxygen to carbon (O : C) and hydrogen to carbon (H : C). The HR-TOF-AMS is limited in aerosol size range, ~50–~600 nm as a result of the aerodynamic lens,[43] the composition of the aerosols is assumed to remain the same regardless of size and the total compositional mass is thus determined using eqn (1)

$$m_x = m \times \frac{x}{\text{org} + \text{NO}_3 + \text{NH}_4 + \text{SO}_4} \quad (1)$$

where m_x is the total aerosol mass of species x. Org, NO_3, NH_4, and SO_4 are the mass of the respective species determined by the AMS, x is equal to one of four species. m is the total aerosol mass determined by the SMPS, assuming a density of 1.6 g cm^{-3} determined by APM.

Secondary Organic Carbon (SOC) was calculated based on m_x and the organic matter to organic carbon ratio (OM/OC).

$$\text{SOC} = \frac{m_{\text{org}}}{\text{OM/OC}} \quad (2)$$

The potential SOC mass of compound x ($SOCP_x$) is calculated based on the losses of aromatic gas phase compounds measured by REMPI-MS.

$$SOCP_x = \Delta X \times \frac{C_x}{M_x} \quad (3)$$

where ΔX is the difference in concentration in mg m^{-3} of compound X before and after aging in the PEAR and C_x is the ratio of carbon weight to the molecular weight M_x of compound X.

Emission factor calculation

The emission factor (EF) is calculated to represent the PM emitted and SOA formed as mg per distance driven (mg km^{-1}) or mg per kg fuel consumed (mg kg^{-1}). The fuel consumption and distance driven were tracked online by the vehicle on-board diagnostics and the dynamometer, respectively. Emission factors were then calculated as in eqn (4).

$$EF = \frac{C \times Q_{dry}}{F} \quad (4)$$

where EF is the emission factor, C is the concentration in milligrams per cubic meter, Q_{dry} is the volume of the dry exhaust from the car in cubic meters per second and F is either the fuel consumption in kg per second or the distance driven in kilometres per second (S1.1†).

Results and discussion

In the primary emissions, aerosol number concentrations (electrical mobility diameter >10 nm) appeared close to the limit of detection throughout the driving cycle, an expected effect from the GPF (Fig. 2A). Therefore, there is a distinct improvement in primary aerosol emission reduction compared to previous studies on Euro 6 cars[44] and especially an improvement compared to Euro 5 primary emissions[11,25,45] without GPF. One other study has reported comparable reductions by retrofitting a modern GPF to a Euro 5 compliant GDI vehicle.[16]

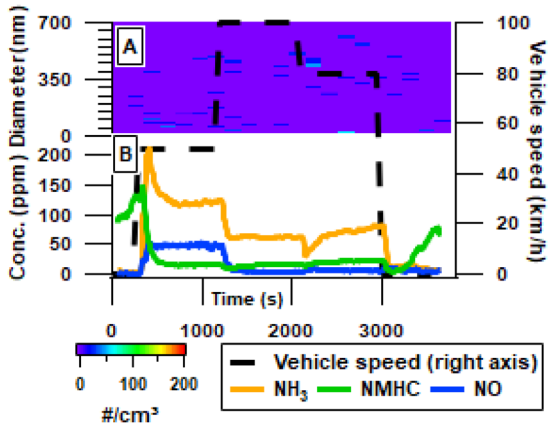

Fig. 2 Time resolved fresh emissions of number concentration measured by SMPS (A), and gas phase emissions measured by FTIR in ppm (B). Concentrations are provided at tailpipe levels.

However, it has been shown that GDI vehicles with no GPF emit primary aerosols in the 3–10 nm diameter range,[44] such nanoparticles are however outside the accessible measurement range of the used SMPS. In contrast to the reduction of aerosols, inorganic and organic gases were detected with dynamic concentrations throughout the driving cycle (Fig. 2B). During warm idling, emissions are dominated by NMHC, and these emissions reach maximum at the initial acceleration from idling to 50 km h^{-1}. This coincides with a sharp rise of NH_3, which had a concentration of 4.1 ± 0.6 ppm during idling. Emissions of NMHC remained relatively stable during the driving phase and varied only between 10 and 25 ppm upon acceleration or deceleration. Throughout the driving phase NH_3 remains the largest emission, disregarding CO and CO_2. High NH_3 emissions are a direct result of the TWC, and forms due to the H_2 produced in the CO to CO_2 reaction. The higher H_2 concentration thus interferes in the catalytic reaction intended to convert NO_x to N_2 and instead forms NH_3. This increase in NH_3 was reported to be up to 72 times the NH_3 emissions without the TWC.[19] At speeds of 100 km h^{-1} and 80 km h^{-1} only low amounts of NO (5.3 ± 1.2 ppm) were detected indicating efficient removal of NO during these speeds. However, at a speed of 50 km h^{-1}, a significant amount of NO (47.1 ± 3.1 ppm) is not converted to N_2 or NH_3. Particularly at speed 50 km h^{-1} the NO concentrations exceed the level of NMHC, changing the oxidation pathways and composition of the aerosol significantly.

Fig. 3A illustrates the 3 largest VOC groups as measured by PTR-MS, with benzene emitted at comparable levels to all other

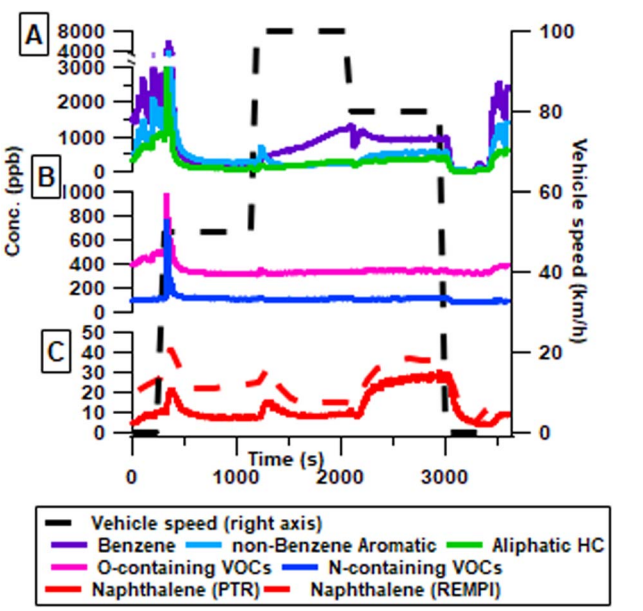

Fig. 3 VOC concentrations measured with PTR (solid lines) over the average driving cycle (N = 9) for primary emissions at tail pipe concentrations. (A) shows benzene, non-benzene aromatic and the combined aliphatic hydrocarbon. (B) shows both oxygen containing VOCs and nitrogen containing VOCs. (C) shows the time series of the aromatic compound naphthalene as measured with both, PTR and REMPI (n = 12).

aromatics combined. However, during 100 and 80 km h^{-1} the benzene emissions are the highest contribution to the total VOC. Aliphatic hydrocarbon (HC) is at a similar level to the non-benzene aromatic, throughout the driving cycle. The non-benzene aromatics consist of toluene, o-/m-/p-xylene or ethylbenzene, C3-benzenes, C4-benzenes, naphthalene, styrene and methyl styrene primarily, this is similar to the composition found in previous papers that reported these compounds plus benzene as 96.7% of total aromatic hydrocarbon and 69.5% of total non-methane organic carbon.[11] Previous papers have reported significant gas phase poly aromatic hydrocarbons (PAHs) with offline instrumentation, however no 3+ ringed PAHs were observed in this study with online instrumentation.[15,29] The main peak for all major groups is found during acceleration to 50 km h^{-1} after 15 min of idling. As idling starts after driving a drop in all VOCs occurs for 5 minutes after which there is a rapid increase in all major components. The same trends are significant for oxygen containing and nitrogen containing VOCs (Fig. 3B). The sudden and sharp rise in aromatic and aliphatic HC stands in contrast to the more gradual increase of NMHCs starting after only 2 minutes. This could indicate that some smaller non-polar compounds which are not detectable by the PTR-MS are emitted from the car earlier than the larger compounds potentially because of the cooling of the engine. Independent measurements of VOCs with aromatic functionalities by REMPI-ToF-MS and PTR-ToF-MS showed similar trends (exemplarily shown for naphthalene in Fig. 3C); REMPI-TOFMS consistently measured higher concentration than the PTR-MS, which may be related to the uncertainty of the photoionization cross-section.[41] Furthermore, analysis of aromatics was performed with the REMPI-MS as it alternated between measuring fresh emissions and aged emissions.

Formation of secondary aerosol

Substantial aerosol formation was observed after oxidation by OH of the exhaust emission equivalent to 2.2 days, assuming an ambient OH concentration of 10^6 cm^{-3} (Fig. 4A). The secondary aerosol had an electrical mobility diameter below 100 nm, with a geometric mean diameter of 36 ± 3 nm, a mass geometric mean of 88 ± 9 nm, and a driving condition-dependent size distribution, which showed the largest size mode during acceleration from idling to 50 km h^{-1}. The mass concentration for aerosols below 100 nm was determined by incorporating the aerosol density of 1.6 ± 0.1 g cm^{-3} derived from APM measurements (Fig. 4B). The highest short-term concentrations occur during accelerations and the highest stable concentrations are observed at 50 km h^{-1}. The total concentrations of secondary aerosol formed during 80 and 100 km h^{-1} remain stable. In order to predict if SOA is formed from unburned fuel or incomplete combustion the SOA/CO ratio can be used, as CO is only formed in incomplete combustion. Thus a high SOA/CO ratio would indicate that SOA formation occurs as a result of unburned fuel, whereas a low SOA/CO indicates that the SOA formed is associated with incomplete combustion. The SOA/CO ratio (Fig. 4B) shows a significant change throughout all driving speeds, with idling SOA/CO reaching 729 μg ppm^{-1}, indicating that the SOA is formed primarily from unburned fuel. At increasing speed the SOA/CO ratio decreases suggesting a transition to incomplete combustion away from unburned fuel. This aligns well with the observations made in the literature.[17]

Throughout the driving phase the O : C and H : C remained stable between 0.93–1.03 ± 0.02 and 0.99–1.08 ± 0.01 respectively. The highest O : C ratio was found during 100 km h^{-1} and the lowest during 50 km h^{-1}, inverse for H : C (Table S10†). These changes suggest a stable oxidation process during the steady state driving. However, the composition of the aerosol changes between 100 km h^{-1} and 80 km h^{-1} as the OM to NO_3 ratio changes from 1.85 ± 0.7 to 3.38 ± 0.06 (Fig. 4B). Maximum concentrations of organic aerosol and nitrate can be measured during accelerations, particularly going from idling to 50 km h^{-1}, resulting in a primarily large increase in the organic aerosol concentration, fitting to gas phase analysis previously discussed regarding the primary emissions. At the onset of warm idling after driving 80 km h^{-1}, the aerosol concentration decreases, and the composition changes from organic-rich (Org : NO_3 3.38 ± 0.06) to nitrate-rich aerosol (Org : NO_3 0.23 ± 0.03). This period of low SOA formation coincided with low NHMC emissions of less than 10 ppm for approximately 3 minutes (Fig. 2B). Thus, idling at, *e.g.*, red lights or short idling in general traffic are typical periods with low organic aerosol formation. However, inorganic SA formation is increased during warm idling. For idling times longer than 3 minutes, however, NMHC emissions significantly increased resulting in enhanced SOA formation which may be a consequence of the enhanced release of alkanes from lubrication oil.[46,47] After 5 to 6 minutes of idling, the aerosol composition turns organic-rich (org : NO_3 > 10), which agrees with higher HC emissions than NO emissions in a previous study on idling emissions from gasoline cars.[48] The nitrate concentration throughout the driving cycle follows the trend of NH_4 with an average ratio of 2.5 ± 0.3, suggesting that nucleation of ammonium nitrate (AN) is limited by the concentration of NO_3, and therefore that most aerosol phase NO_3 is AN bound. The relatively high concentrations of NH_3 remain unaffected after exposure to OH and O_3, while the concentration of aerosol phase nitrate increased by the oxidation of NO and NO_2. This follows the expected reaction pathway of $NO_2 + OH \rightarrow HNO_3$ which reacts rapidly with NH_3 to form NH_4NO_3(s). As NH_3 is available in large quantities the conversion of NO_x to HNO_3 is the limiting factor in this experiment. The secondary production of AN during driving enhances aerosol formation, observed in this experiment as it provides a condensation sink and overcomes the nucleation boundary for oxidized organic vapours, allowing for condensable gas phase oxidation products to partition to the aerosol phase.

Secondary aerosol precursors

SOC was calculated using eqn (2) and compared with potential SOC formed from aromatics measured by REMPI according to eqn (3) (Fig. 5). Determination of SOC was used alternatively to SOA as calculating SOA formation from the initial VOCs requires accurate knowledge of the individual SOA yields, for

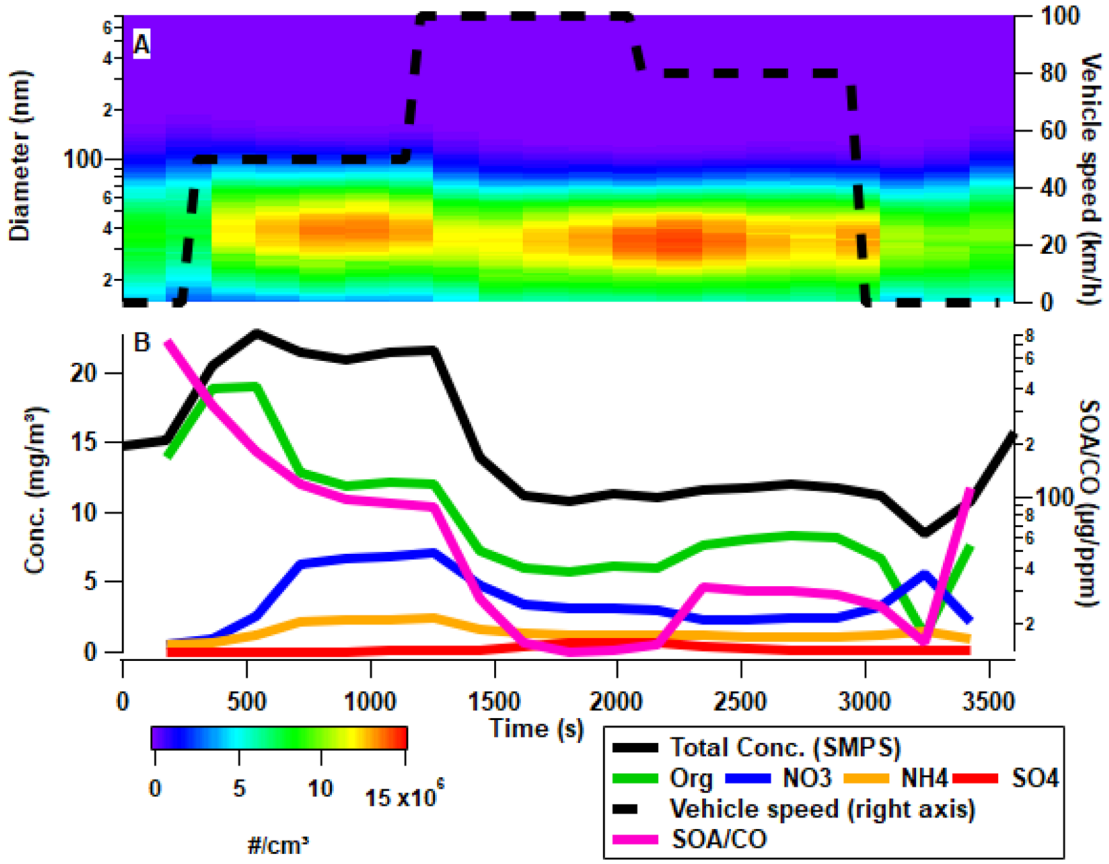

Fig. 4 The vehicle speed is shown on the right axis and illustrates the driving conditions. (A) Average ($n = 12$) aerosol number concentration at the tailpipe. (B) Average ($n = 12$) aerosol mass concentration at the tailpipe derived from SMPS assuming a density of 1.6 g cm^{-3} and the secondary organic aerosol measured by AMS.

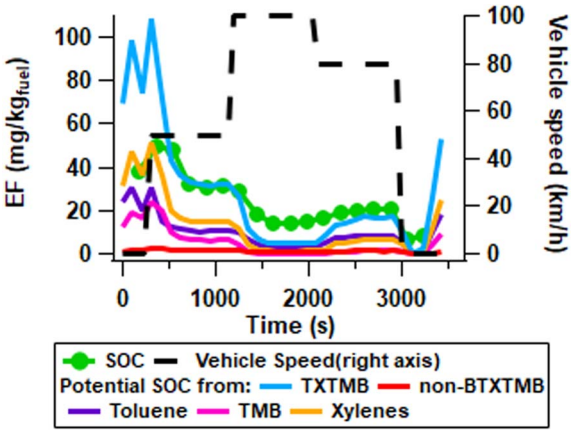

Fig. 5 Secondary organic carbon (SOC) as calculated in eqn (2) and converted to mg aerosol per kg fuel, compared with potential SOC mass derived from measured aromatics by REMPI and eqn (3). Toluene, xylene and trimethyl-benzene (TXTMB) are the most important sources of SOC covering 99% of the total aromatic SOC potential ($n = 12$).

each precursor and mixtures thereof. Due to the high VOC concentrations in the PEAR and high NH_3 conditions, which potentially increases the SOA yield, literature SOA yields would likely underestimate the SOA mass formed.[11,20,49,50] The SOC potential indicates the highest possible SOC that could be formed based on the total conversion of lost aromatic carbon mass from the gas phase to the aerosol phase. Among all aromatic VOCs 99% of the total aromatic SOC potential results only from toluene, xylene and trimethyl-benzene (TXTMB). TXTMB follows the SOA/CO ratio displayed in Fig. 4B. This implies that unburned fuel dominates SOA formation at lower vehicle speeds, however at 100 km h^{-1} the SOA formation is driven by incomplete combustion. It should be noted that during incomplete combustion aromatic formation can occur in the engine as a result of pyrosynthesis.[51] PTR-MS was analysed, and the main components were found to be propyne and butene (Table S12†). However, with emissions <9 mg kg^{-1}, and low SOA yields, these compounds' expected SOA formation contribution are considered low. FTIR measured emissions of hexane and pentane above 490 mg kg^{-1} during idling (Table S13†). The highest emission of a single aliphatic NMHC was hexane, regardless of vehicular speed. Due to the concentrations in the PEAR, hexane could be a significant SOA precursor. Previous papers have reported similarly that TXTMB account for the majority of reacted aromatics.[11] During idling the SOC potential from TXTMB was found to be much higher than the SOC formed. This loss of carbon is expected as the potential

assumes a conversion of unity from the gas phase to the aerosol, whilst the SOA yield likely is higher in the PEAR than would be expected in the atmosphere due to higher concentrations of organics and AN particle formation during driving. Additionally, there are losses by photolysis at 254 nm (Table S8†), further there is no AN formation during idling which likely decreases the amount of VOCs that partition to the particle phase through oxidation. During 50 and 80 km h^{-1}, the levels of potential SOC from TXTMB and the measured SOC are comparable. However, there are likely other sources that contribute to the SOC formation. This is evident in the 100 km h^{-1} driving phase where the TXTMB SOC potential is only sufficient to explain 50% of the formed SOC. Other notable aromatics that may affect SOC formation can be naphthalene and benzene. Whilst naphthalene concentration was reduced after aging as would be expected from its high SOA yield[52] the concentrations are too low to have significant impact on the potential SOC formation. In contrast, benzene was the most abundant aromatic compound in the exhaust. However, there is no observed reduction in benzene concentration as a result of aging in the PEAR, due to its slow reaction rate with OH ($k(298\ K) = 1.22 \times 10^{-12}$ cm^3 per molecule per s).[53] Similarly very low reduction in benzene at a low atmospheric age was observed by Pieber *et al.* 2018.[11] TMB was observed to impact the potential SOC primarily during idling and 50 km h^{-1} where it accounts for 19–30%, whereas during the 80 and 100 km h^{-1} driving conditions the contribution was between 4 and 10% of the potential TXTMB SOC. This trend is comparable to that of xylene which is the main source of potential aromatic SOC during idling and 50 km h^{-1} accounting for 45–50% of the potential SOC from TXTMB. This decreased to 15–40% during 80 and 100 km h^{-1}, at these driving speeds toluene accounts for up to 80% of the total aromatic potential SOC. These results indicate that as driving speeds increase the share of aromatic SOC from toluene increases, as well. However, the importance of aromatics on SOC decreases as driving speed increases, suggesting that SOC formed from other sources such as long chained alkanes or polyaromatic hydrocarbons is more important at higher driving speeds. Yang *et al.* 2018 suggested that there should still be significant PAHs in the gas-phase though it was found that the GPF reduced the PAH emissions.[15]

However, with the online instrumentation used in this experiment, it was not possible to observe any significant concentration of long chained alkanes or PAHs.

Emission factors

To compare the emissions observed with previous studies and emission standard limits, emission factors (EFs) are calculated based on eqn (4). The average aerosol EFs (Fig. 6) refer to steady state driving defined as the condition reached after cruising at a speed for more than 5 minutes, which was chosen to avoid the influence of accelerations (Fig. 4B). Secondary organic aerosol mass per kilogram fuel decreased with increasing vehicle speed (Fig. 6), which suggests an increased engine combustion or TWC conversion efficiency at higher driving speeds within the range of 50 to 100 km h^{-1}. Under faster steady state driving

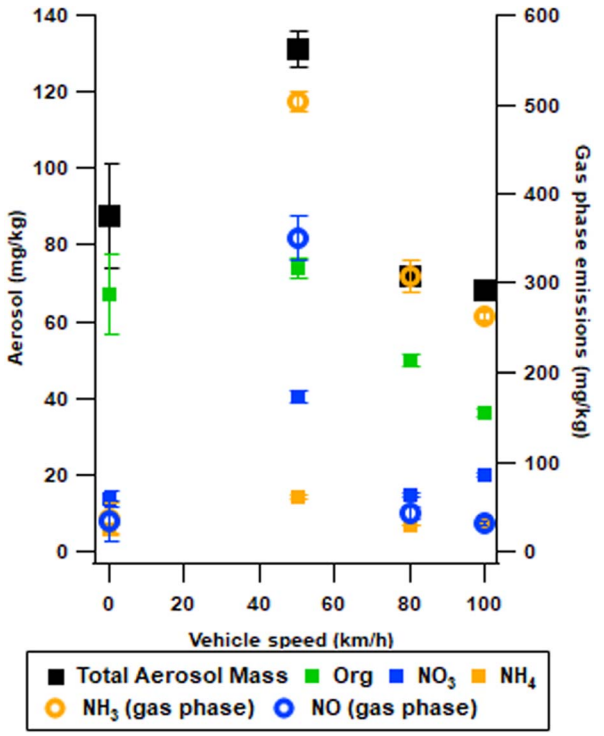

Fig. 6 Emission factors in mg per kg fuel. Squares illustrate the particle phase, circles the gas phase constituents. Each point is the average value for each speed measured for 10 min of each driving cycle ($n = 12$) and error bars are the standard deviation.

conditions, which are more relevant for highway cruising emissions, the observed trend between speed and EFs may change. Furthermore, slower driving conditions such as residential zone driving should not be directly compared with steady state driving. The total aerosol mass formed is highest at 50 km h^{-1} reaching 131 ± 5 mg kg^{-1}, compared to 68 ± 1 mg kg^{-1} and 72 ± 2 mg kg^{-1} for speeds of 100 and 80 km h^{-1}, respectively. However, at a speed of 100 km h^{-1}, SOA formation accounted for 36 ± 1 mg kg^{-1}, that is, 54% of the total aerosol mass, in comparison to 50 ± 1 mg kg^{-1}, that is, 69% of the total aerosol mass, at a speed of 80 km h^{-1}. Moreover, gas phase NH_3 and NO emissions are the highest at 50 km h^{-1}, but lowest when driving 100 km h^{-1}. For EFs of secondary nitrate, the trend with speed differs from SOA as it slightly increases at 100 km h^{-1}. It is worth noting that the formation of AN aerosol might function as an effective seed particle for the organics to condense on increasing the SOA yield when AN is high.

Roth *et al.* 2019 found a similar composition of the aerosol with a Euro 5 retrofitted with a GPF, with SOA forming roughly 50% of the secondary aerosol mass and ammonium nitrate forming the remaining 50% of the total secondary aerosol.[16] Pieber *et al.* 2018 (ref. 11) with retrofitted GPF on Euro 5 found that in SOA and nitrate SA was similar in concentrations and thus that SOA accounted for less than 50% of total SOA when operating in a smog chamber. However, in an OFR similar levels were observed at low atmospheric ages with SOA accounting for roughly 50% of total SA, with the share of SOA increasing with

increasing atmospheric age.[11] Zhang *et al.* 2023 reported lower SOA formation from China VI cars at cruising speeds between 30 and 60 km h^{-1}, however they saw a significant increase in SOA as speeds increased beyond 60 km h^{-1}. Additionally, the idling SOA formation is comparable between China VI and Euro 6d.[17]

These results are comparable despite the clear differences in driving cycle with cold started LA92 and WLTC used by Roth *et al.* 2019 [16] and Pieber *et al.* 2018 [11] respectively compared to the hot start steady state driving presented in this study and Zhang *et al.* 2023.[17]

Emission standards for cars, such as the Euro 6, are given in mg per km driven. The Euro 6 limits particulate matter to 4.5 mg km^{-1}. With the introduction of the GPF emission of primary aerosols is well below this limit. However, there is still significant aerosol formation after aging, during 50 km h^{-1} secondary aerosols reach 5.1 mg km^{-1} during the steady state (Table S4†).

Generally, more dynamic driving in the real world and more dynamic driving cycles, such as WLTP, may lead to higher emissions of SOA precursors,[44] hence the results denote a lower limit. Furthermore, NH_3 enhances SOA yields and new particle formation under high concentrations,[20,25] and thus introducing cars with increased NH_3 emissions to urban centres would enhance particle nucleation and thus the formation of secondary ultrafine particles, although the high surface area of condensation sinks in an urban environment.[54] Moreover, NH_3 can further react with additional species nucleating into the aerosol for SOA from other sources as well.[55] It is well known that idling conditions have large emissions of organics,[25] which may form large amounts of SOA. In this study, the mass of SOA formed was lower during idling than at a speed of 50 km h^{-1}. This is likely linked to the NO emissions, during 50 km h^{-1} forming AN particles. The AN particles function as seed particles for organic compounds allowing condensation of organic matter. Thus, the SOA from idling might be underestimated due to low AN formation during this phase.

Conclusions

The results demonstrate the efficiency of the GPF, reducing primary aerosol mass to close to zero. However, the removal of primary aerosol does not limit the formation of secondary aerosol from the remaining VOCs in the exhaust of gasoline cars. Particularly, aromatic VOCs, TXTMB, originating either from unburned fuel or pyro synthesis *via* radical reactions, and NO_x are potent precursors of secondary aerosols. Once released to the atmosphere, oxidative gas-to-particle photochemical conversion leads to SOA and secondary nitrate formation. The observed SOA formation cannot be completely explained by the TXTMB and thus an additional VOC precursor must exist. However, PTR-MS and FTIR-MS were unable to identify species that would give closure to the SOA formation. Only during idling could the TXTMB account for the total observed SOA, this further suggests that these compounds are linked to unburned fuel. Moreover, gasoline cars equipped with a TWC may be a significant source of NH_3. Furthermore, with the incomplete conversion of NO_x emissions in the TWC along with the high NH_3 emissions, the TWC equipped cars also become a source of secondary inorganic aerosol due to the production of ammonium nitrates in the atmosphere. Therefore, attempts to reduce aromatic VOC, NO_x and NH_3 are most promising to further reduce tailpipe emissions from gasoline cars which lead to significant secondary aerosol formation.

Current regulation standards in the European union, Euro 6d, have no restrictions for aromatic VOCs or NH_3. Even though the aromatic VOCs are indirectly restricted through total NMHCs, it could be possible to reduce NMHC without affecting the SOA formation as the composition of the NMHC has a significant impact on SOA formation. The proposed Euro 7 would restrict NH_3 emissions, and thus the implementation of such legislation would likely improve air quality.

Author contributions

Andreas Paul: conceptualization, investigation, formal analysis, methodology, visualization, and writing – original draft. Zheng Fang: investigation, and writing – review & editing. Patrick Martens: investigation, and writing – review & editing. Arya Mukherjee: investigation, and writing – review & editing. Gert Jakobi: investigation and methodology. Mika Ihalainen: investigation, methodology and writing – original draft. Miika Kortelainen: investigation. Markus Somero: investigation. Pasi Yli-Pirilä: investigation. Thorsten Hohaus: conceptualization, supervision, and writing – review & editing. Hendryk Czech: conceptualization, investigation, project administration, supervision, and writing – review & editing. Markus Kalberer: resources, supervision, and writing – review & editing. Olli Sippula: funding acquisition, project administration, resources, supervision, and writing – review & editing. Yinon Rudich: funding acquisition, resources, supervision, and writing – review & editing. Ralf Zimmermann: funding acquisition, resources, supervision, and writing – review & editing. Astrid Kiendler-Scharr: funding acquisition, and supervision.

Conflicts of interest

There are no conflicts to declare.

Acknowledgements

We thank the Helmholtz International Laboratory AeroHEALTH (InterLabs-0005; **https://aerohealth.eu**) and the ULTRHAS Horizon Europe project (agreement 955390) for supporting this work.

References

1 O. World Health, *Ambient Air Pollution: A Global Assessment of Exposure and Burden of Disease*, World Health Organization, Geneva, 2016.
2 J. Lelieveld, A. Pozzer, U. Pöschl, M. Fnais, A. Haines and T. Münzel, Loss of life expectancy from air pollution

compared to other risk factors: a worldwide perspective, *Cardiovasc. Res.*, 2020, **116**(11), 1910–1917.

3 C. J. L. Murray, Global burden of 87 risk factors in 204 countries and territories, 1990–2019: a systematic analysis for the Global Burden of Disease Study 2019, *Lancet*, 2020, **396**(10258), 1223–1249.

4 H. O. T. Pye, C. K. Ward-Caviness, B. N. Murphy, K. W. Appel and K. M. Seltzer, Secondary organic aerosol association with cardiorespiratory disease mortality in the United States, *Nat. Commun.*, 2021, **12**(1), 7215.

5 S. Offer, E. Hartner, S. Di Bucchianico, C. Bisig, S. Bauer, J. Pantzke, J. Zimmermann Elias, X. Cao, S. Binder, E. Kuhn, A. Huber, S. Jeong, U. Käfer, P. Martens, A. Mesceriakovas, J. Bendl, R. Brejcha, A. Buchholz, D. Gat, T. Hohaus, N. Rastak, G. Jakobi, M. Kalberer, T. Kanashova, Y. Hu, C. Ogris, A. Marsico, F. Theis, M. Pardo, T. Gröger, S. Oeder, J. Orasche, A. Paul, T. Ziehm, Z.-H. Zhang, T. Adam, O. Sippula, M. Sklorz, J. Schnelle-Kreis, H. Czech, A. Kiendler-Scharr, Y. Rudich and R. Zimmermann, Effect of Atmospheric Aging on Soot Particle Toxicity in Lung Cell Models at the Air–Liquid Interface: Differential Toxicological Impacts of Biogenic and Anthropogenic Secondary Organic Aerosols (SOAs), *Environ. Health Perspect.*, 2022, **130**(2), 027003.

6 S. Edwards, G. Zhao, J. Tran, K. T. Patten, A. Valenzuela, C. Wallis, K. J. Bein, A. S. Wexler, P. J. Lein and X. Rao, Pathological Cardiopulmonary Evaluation of Rats Chronically Exposed to Traffic-Related Air Pollution, *Environ. Health Perspect.*, 2020, **128**(12), 127003.

7 J. A. Holme, B. C. Brinchmann, M. Refsnes, M. Låg and J. Øvrevik, Potential role of polycyclic aromatic hydrocarbons as mediators of cardiovascular effects from combustion particles, *Environ. Health*, 2019, **18**(1), 74.

8 A. Joshi and T. V. Johnson, Gasoline Particulate Filters—a Review, *Emiss. Control Sci. Technol.*, 2018, **4**(4), 219–239.

9 D. R. Gentner, S. H. Jathar, T. D. Gordon, R. Bahreini, D. A. Day, I. El Haddad, P. L. Hayes, S. M. Pieber, S. M. Platt, J. de Gouw, A. H. Goldstein, R. A. Harley, J. L. Jimenez, A. S. H. Prévôt and A. L. Robinson, Review of Urban Secondary Organic Aerosol Formation from Gasoline and Diesel Motor Vehicle Emissions, *Environ. Sci. Technol.*, 2017, **51**(3), 1074–1093.

10 Y. Morino, Y. Li, Y. Fujitani, K. Sato, S. Inomata, K. Tanabe, S. H. Jathar, Y. Kondo, T. Nakayama, A. Fushimi, A. Takami and S. Kobayashi, Secondary organic aerosol formation from gasoline and diesel vehicle exhaust under light and dark conditions, *Environ. Sci.: Atmos.*, 2022, **2**(1), 46–64.

11 S. M. Pieber, N. K. Kumar, F. Klein, P. Comte, D. Bhattu, J. Dommen, E. A. Bruns, D. Kılıç, I. El Haddad, A. Keller, J. Czerwinski, N. Heeb, U. Baltensperger, J. G. Slowik and A. S. H. Prévôt, Gas-phase composition and secondary organic aerosol formation from standard and particle filter-retrofitted gasoline direct injection vehicles investigated in a batch and flow reactor, *Atmos. Chem. Phys.*, 2018, **18**(13), 9929–9954.

12 Y. Zhao, A. T. Lambe, R. Saleh, G. Saliba and A. L. Robinson, Secondary Organic Aerosol Production from Gasoline Vehicle Exhaust: Effects of Engine Technology, Cold Start, and Emission Certification Standard, *Environ. Sci. Technol.*, 2018, **52**(3), 1253–1261.

13 E. Z. Nordin, A. C. Eriksson, P. Roldin, P. T. Nilsson, J. E. Carlsson, M. K. Kajos, H. Hellén, C. Wittbom, J. Rissler, J. Löndahl, E. Swietlicki, B. Svenningsson, M. Bohgard, M. Kulmala, M. Hallquist and J. H. Pagels, Secondary organic aerosol formation from idling gasoline passenger vehicle emissions investigated in a smog chamber, *Atmos. Chem. Phys.*, 2013, **13**(12), 6101–6116.

14 T. Liu, X. Wang, W. Deng, Q. Hu, X. Ding, Y. Zhang, Q. He, Z. Zhang, S. Lü, X. Bi, J. Chen and J. Yu, Secondary organic aerosol formation from photochemical aging of light-duty gasoline vehicle exhausts in a smog chamber, *Atmos. Chem. Phys.*, 2015, **15**(15), 9049–9062.

15 J. Yang, P. Roth, T. D. Durbin, K. C. Johnson, D. R. Cocker III, A. Asa-Awuku, R. Brezny, M. Geller and G. Karavalakis, Gasoline Particulate Filters as an Effective Tool to Reduce Particulate and Polycyclic Aromatic Hydrocarbon Emissions from Gasoline Direct Injection (GDI) Vehicles: A Case Study with Two GDI Vehicles, *Environ. Sci. Technol.*, 2018, **52**(5), 3275–3284.

16 P. Roth, J. Yang, E. Fofie, D. R. Cocker III, T. D. Durbin, R. Brezny, M. Geller, A. Asa-Awuku and G. Karavalakis, Catalyzed Gasoline Particulate Filters Reduce Secondary Organic Aerosol Production from Gasoline Direct Injection Vehicles, *Environ. Sci. Technol.*, 2019, **53**(6), 3037–3047.

17 J. Zhang, J. Peng, A. Song, Z. Lv, H. Tong, Z. Du, J. Guo, L. Wu, T. Wang, M. Hallquist and H. Mao, Marked impacts of transient conditions on potential secondary organic aerosol production during rapid oxidation of gasoline exhausts, *npj Clim. Atmos. Sci.*, 2023, **6**(1), 59.

18 P. K. Hopke and X. Querol, Is Improved Vehicular NOx Control Leading to Increased Urban NH3 Emissions?, *Environ. Sci. Technol.*, 2022, **56**(17), 11926–11927.

19 Y. Liu, Y. Ge, J. Tan, H. Wang and Y. Ding, Research on ammonia emissions characteristics from light-duty gasoline vehicles, *J. Environ. Sci.*, 2021, **106**, 182–193.

20 S. Liu, D. Huang, Y. Wang, S. Zhang, X. Liu, C. Wu, W. Du and G. Wang, Synergetic effects of NH3 and NOx on the production and optical absorption of secondary organic aerosol formation from toluene photooxidation, *Atmos. Chem. Phys.*, 2021, **21**(23), 17759–17773.

21 K. Li, L. Chen, S. J. White, H. Yu, X. Wu, X. Gao, M. Azzi and K. Cen, Smog chamber study of the role of NH3 in new particle formation from photo-oxidation of aromatic hydrocarbons, *Sci. Total Environ.*, 2018, **619–620**, 927–937.

22 M. Wang, W. Kong, R. Marten, X.-C. He, D. Chen, J. Pfeifer, A. Heitto, J. Kontkanen, L. Dada, A. Kürten, T. Yli-Juuti, H. E. Manninen, S. Amanatidis, A. Amorim, R. Baalbaki, A. Baccarini, D. M. Bell, B. Bertozzi, S. Bräkling, S. Brilke, L. C. Murillo, R. Chiu, B. Chu, L.-P. De Menezes, J. Duplissy, H. Finkenzeller, L. G. Carracedo, M. Granzin, R. Guida, A. Hansel, V. Hofbauer, J. Krechmer, K. Lehtipalo, H. Lamkaddam, M. Lampimäki, C. P. Lee, V. Makhmutov, G. Marie, S. Mathot, R. L. Mauldin, B. Mentler, T. Müller, A. Onnela, E. Partoll, T. Petäjä,

M. Philippov, V. Pospisilova, A. Ranjithkumar, M. Rissanen, B. Rörup, W. Scholz, J. Shen, M. Simon, M. Sipilä, G. Steiner, D. Stolzenburg, Y. J. Tham, A. Tomé, A. C. Wagner, D. S. Wang, Y. Wang, S. K. Weber, P. M. Winkler, P. J. Wlasits, Y. Wu, M. Xiao, Q. Ye, M. Zauner-Wieczorek, X. Zhou, R. Volkamer, I. Riipinen, J. Dommen, J. Curtius, U. Baltensperger, M. Kulmala, D. R. Worsnop, J. Kirkby, J. H. Seinfeld, I. El-Haddad, R. C. a. Flagan and N. M. Donahue, Rapid growth of new atmospheric particles by nitric acid and ammonia condensation, *Nature*, 2020, **581**(7807), 184–189.

23 R. Suarez-Bertoa, M. Pechout, M. Vojtíšek and C. Astorga, Regulated and Non-Regulated Emissions from Euro 6 Diesel, Gasoline and CNG Vehicles under Real-World Driving Conditions, *Atmosphere*, 2020, **11**(2), 204.

24 EU, COM(2022) 586 Final Regulation Of The European Parliament and of The Council on type-approval of motor vehicles and engines and of systems, components and separate technical units intended for such vehicles, with respect to their emissions and battery durability (Euro 7) and repealing regulations (EC) No. 715/2007 and (EC) No. 595/2009: 2022.

25 H. Wang, S. Guo, Y. Yu, R. Shen, W. Zhu, R. Tang, R. Tan, K. Liu, K. Song, W. Zhang, Z. Zhang, S. Shuai, H. Xu, J. Zheng, S. Chen, S. Li, L. Zeng and Z. Wu, Secondary aerosol formation from a Chinese gasoline vehicle: Impacts of fuel (E10, gasoline) and driving conditions (idling, cruising), *Sci. Total Environ.*, 2021, **795**, 148809.

26 E. Kostenidou, A. Martinez-Valiente, B. R'Mili, B. Marques, B. Temime-Roussel, A. Durand, M. André, Y. Liu, C. Louis, B. Vansevenant, D. Ferry, C. Laffon, P. Parent and B. D'Anna, Technical note: Emission factors, chemical composition, and morphology of particles emitted from Euro 5 diesel and gasoline light-duty vehicles during transient cycles, *Atmos. Chem. Phys.*, 2021, **21**(6), 4779–4796.

27 L. Chen, Z. Liang, X. Zhang and S. Shuai, Characterizing particulate matter emissions from GDI and PFI vehicles under transient and cold start conditions, *Fuel*, 2017, **189**, 131–140.

28 A. H. Hartikainen, M. Ihalainen, P. Yli-Pirilä, L. Hao, M. Kortelainen, S. M. Pieber and O. Sippula, Photochemical transformation and secondary aerosol formation potential of Euro6 gasoline and diesel passenger car exhaust emissions, *J. Aerosol Sci.*, 2023, **171**, 106159.

29 Y. Zhao, R. Saleh, G. Saliba, A. A. Presto, T. D. Gordon, G. T. Drozd, A. H. Goldstein, N. M. Donahue and A. L. Robinson, Reducing secondary organic aerosol formation from gasoline vehicle exhaust, *Proc. Natl. Acad. Sci. U. S. A.*, 2017, **114**(27), 6984–6989.

30 M. Ihalainen, P. Tiitta, H. Czech, P. Yli-Pirilä, A. Hartikainen, M. Kortelainen, J. Tissari, B. Stengel, M. Sklorz, H. Suhonen, H. Lamberg, A. Leskinen, A. Kiendler-Scharr, H. Harndorf, R. Zimmermann, J. Jokiniemi and O. Sippula, A novel high-volume Photochemical Emission Aging flow tube Reactor (PEAR), *Aerosol Sci. Technol.*, 2019, **53**(3), 276–294.

31 P. Barmet, J. Dommen, P. F. DeCarlo, T. Tritscher, A. P. Praplan, S. M. Platt, A. S. H. Prévôt, N. M. Donahue and U. Baltensperger, OH clock determination by proton transfer reaction mass spectrometry at an environmental chamber, *Atmos. Meas. Tech.*, 2012, **5**(3), 647–656.

32 A. Allani, Y. Bedjanian, D. K. Papanastasiou and M. N. Romanias, Reaction Rate Coefficient of OH Radicals with d9-Butanol as a Function of Temperature, *ACS Omega*, 2021, **6**(28), 18123–18134.

33 P. L. Hayes, A. M. Ortega, M. J. Cubison, K. D. Froyd, Y. Zhao, S. S. Cliff, W. W. Hu, D. W. Toohey, J. H. Flynn, B. L. Lefer, N. Grossberg, S. Alvarez, B. Rappenglück, J. W. Taylor, J. D. Allan, J. S. Holloway, J. B. Gilman, W. C. Kuster, J. A. de Gouw, P. Massoli, X. Zhang, J. Liu, R. J. Weber, A. L. Corrigan, L. M. Russell, G. Isaacman, D. R. Worton, N. M. Kreisberg, A. H. Goldstein, R. Thalman, E. M. Waxman, R. Volkamer, Y. H. Lin, J. D. Surratt, T. E. Kleindienst, J. H. Offenberg, S. Dusanter, S. Griffith, P. S. Stevens, J. Brioude, W. M. Angevine and J. L. Jimenez, Organic aerosol composition and sources in Pasadena, California, during the 2010 CalNex campaign, *J. Geophys. Res.: Atmos.*, 2013, **118**(16), 9233–9257.

34 Z. Peng, D. A. Day, A. M. Ortega, B. B. Palm, W. Hu, H. Stark, R. Li, K. Tsigaridis, W. H. Brune and J. L. Jimenez, Non-OH chemistry in oxidation flow reactors for the study of atmospheric chemistry systematically examined by modeling, *Atmos. Chem. Phys.*, 2016, **16**(16), 4283–4305.

35 Z. Peng and J. L. Jimenez, Modeling of the chemistry in oxidation flow reactors with high initial NO, *Atmos. Chem. Phys.*, 2017, **17**(17), 11991–12010.

36 Z. Peng, B. B. Palm, D. A. Day, R. Talukdar, W. Hu, A. T. Lambe, W. H. Brune and J. L. Jimenez, Model Evaluation of New Techniques for Maintaining High-NO Conditions in Oxidation Flow Reactors for the Study of OH-Initiated Atmospheric Chemistry, *ACS Earth Space Chem.*, 2018, **2**(2), 72–86.

37 Z. Peng and J. L. Jimenez, KinSim: A Research-Grade, User-Friendly, Visual Kinetics Simulator for Chemical-Kinetics and Environmental-Chemistry Teaching, *J. Chem. Educ.*, 2019, **96**(4), 806–811.

38 Z. Peng, D. A. Day, H. Stark, R. Li, J. Lee-Taylor, B. B. Palm, W. H. Brune and J. L. Jimenez, HO_x radical chemistry in oxidation flow reactors with low-pressure mercury lamps systematically examined by modeling, *Atmos. Meas. Tech.*, 2015, **8**(11), 4863–4890.

39 T. Streibel, F. Mühlberger, R. Geißler, M. Saraji-Bozorgzad, T. Adam and R. Zimmermann, Influence of sulphur addition on emissions of polycyclic aromatic hydrocarbons during biomass combustion, *Proc. Combust. Inst.*, 2015, **35**(2), 1771–1777.

40 H. Czech, O. Sippula, M. Kortelainen, J. Tissari, C. Radischat, J. Passig, T. Streibel, J. Jokiniemi and R. Zimmermann, On-line analysis of organic emissions from residential wood combustion with single-photon ionisation time-of-flight mass spectrometry (SPI-TOFMS), *Fuel*, 2016, **177**, 334–342.

41 C. Gehm, T. Streibel, J. Passig and R. Zimmermann, Determination of Relative Ionization Cross Sections for Resonance Enhanced Multiphoton Ionization of Polycyclic Aromatic Hydrocarbons, *Appl. Sci.*, 2018, **8**(9), 1617.

42 J. Leskinen, M. Ihalainen, T. Torvela, M. Kortelainen, H. Lamberg, P. Tiitta, G. Jakobi, J. Grigonyte, J. Joutsensaari, O. Sippula, J. Tissari, A. Virtanen, R. Zimmermann and J. Jokiniemi, Effective Density and Morphology of Particles Emitted from Small-Scale Combustion of Various Wood Fuels, *Environ. Sci. Technol.*, 2014, **48**(22), 13298–13306.

43 F. Drewnick, S. S. Hings, P. F. Decarlo, J. T. Jayne, M. Gonin, K. Fuhrer, J. L. Jimenez, K. L. Demerjian, S. Borrmann and D. R. Worsnop, A New Time-of-Flight Aerosol Mass Spectrometer (TOF-AMS)—Instrument Description and First Field Deployment, *Aerosol Sci. Technol.*, 2015, **39**(39), 637–658.

44 P. Simonen, J. Kalliokoski, P. Karjalainen, T. Rönkkö, H. Timonen, S. Saarikoski, M. Aurela, M. Bloss, G. Triantafyllopoulos, A. Kontses, S. Amanatidis, A. Dimaratos, Z. Samaras, J. Keskinen, M. Dal Maso and L. Ntziachristos, Characterization of laboratory and real driving emissions of individual Euro 6 light-duty vehicles – Fresh particles and secondary aerosol formation, *Environ. Pollut.*, 2019, **255**, 113175.

45 Y. Zhang, W. Deng, Q. Hu, Z. Wu, W. Yang, H. Zhang, Z. Wang, Z. Fang, M. Zhu, S. Li, W. Song, X. Ding and X. Wang, Comparison between idling and cruising gasoline vehicles in primary emissions and secondary organic aerosol formation during photochemical ageing, *Sci. Total Environ.*, 2020, **722**, 137934.

46 D. R. Worton, G. Isaacman, D. R. Gentner, T. R. Dallmann, A. W. H. Chan, C. Ruehl, T. W. Kirchstetter, K. R. Wilson, R. A. Harley and A. H. Goldstein, Lubricating Oil Dominates Primary Organic Aerosol Emissions from Motor Vehicles, *Environ. Sci. Technol.*, 2014, **48**(7), 3698–3706.

47 G. Caravaggio, J.-P. Charland, P. Macdonald and L. Graham, n-Alkane Profiles of Engine Lubricating Oil and Particulate Matter by Molecular Sieve Extraction, *Environ. Sci. Technol.*, 2007, **41**, 3697–3701.

48 M. R. Aosaf, Y. Wang and K. Du, Comparison of the emission factors of air pollutants from gasoline, CNG, LPG and diesel fueled vehicles at idle speed, *Environ. Pollut.*, 2022, **305**, 119296.

49 N. L. Ng, J. H. Kroll, A. W. H. Chan, P. S. Chhabra, R. C. Flagan and J. H. Seinfeld, Secondary organic aerosol formation from m-xylene, toluene, and benzene, *Atmos. Chem. Phys.*, 2007, **7**(14), 3909–3922.

50 K. Sato, A. Takami, Y. Kato, T. Seta, Y. Fujitani, T. Hikida, A. Shimono and T. Imamura, AMS and LC/MS analyses of SOA from the photooxidation of benzene and 1,3,5-trimethylbenzene in the presence of NOx: effects of chemical structure on SOA aging, *Atmos. Chem. Phys.*, 2012, **12**(10), 4667–4682.

51 V. Kumar, N. C. Kothiyal, Saruchi, P. Vikas and R. Sharma, Sources, distribution, and health effect of carcinogenic polycyclic aromatic hydrocarbons (PAHs) – current knowledge and future directions, *J. Chin. Adv. Mater. Soc.*, 2016, **4**(4), 302–321.

52 A. W. H. Chan, K. E. Kautzman, P. S. Chhabra, J. D. Surratt, M. N. Chan, J. D. Crounse, A. Kürten, P. O. Wennberg, R. C. Flagan and J. H. Seinfeld, Secondary organic aerosol formation from photooxidation of naphthalene and alkylnaphthalenes: implications for oxidation of intermediate volatility organic compounds (IVOCs), *Atmos. Chem. Phys.*, 2009, **9**(9), 3049–3060.

53 Z. Yang, L. Du, Y. Li and X. Ge, Secondary organic aerosol formation from monocyclic aromatic hydrocarbons: insights from laboratory studies, *Environ. Sci.: Processes Impacts*, 2022, **24**(3), 351–379.

54 S. Tuovinen, J. Kontkanen, J. Jiang and M. Kulmala, Investigating the effectiveness of condensation sink based on heterogeneous nucleation theory, *J. Aerosol Sci.*, 2020, **149**, 105613.

55 M. Shrivastava, O. A. Meinrat, P. Artaxo, H. M. J. Barbosa, L. K. Berg, J. Brito, J. Ching, R. C. Easter, J. Fan, J. D. Fast, Z. Feng, J. D. Fuentes, M. Glasius, A. H. Goldstein, E. G. Alves, H. Gomes, D. Gu, A. Guenther, S. H. Jathar, S. Kim, Y. Liu, S. Lou, S. T. Martin, V. F. McNeil, A. Medeiros, S. S. De Sá, J. E. Shiling, S. R. Springston, R. A. F. Souza, J. A. Thornton, G. Isaacman-VanWertz, L. D. Yee, R. Ynoue, R. A. Zaveri, A. Zelenyuk and C. Zhao, Urban pollution greatly enhances formation of natural aerosols over the Amazon rainforest, *Nat. Commun.*, 2019, **10**(10), 1046.